RNA editing alterations define manifestation of prion diseases

Eirini Kanata, Franc Llorens, Dimitra Dafou, Athanasios Dimitriadis, Katrin Thüne, Konstantinos Xanthopoulos, Nikolaos Bekas, Juan Carlos Espinosa, Matthias Schmitz, Alba Marín-Moreno, et al.

HAL Id: hal-03199348
https://hal.inrae.fr/hal-03199348

Submitted on 24 Apr 2021

RNA editing alterations define manifestation of prion diseases

Eirini Kanata[a,1], Franc Llorens[b,c,d,1], Dimitra Dafou[e,1], Athanasios Dimitriadis[a], Katrin Thüne[d,f], Konstantinos Xanthopoulos[g], Nikolaos Bekas[e], Juan Carlos Espinosa[h], Matthias Schmitz[d,f], Alba Marín-Moreno[h], Vincenzo Capece[i], Orr Shormoni[i], Olivier Andréoletti[j], Stefan Bonn[i], Juan María Torres[h], Isidre Ferrer[b,c,k], Inga Zerr[d,f,2], and Theodoros Sklaviadis[a,2,3]

[a]Neurodegenerative Diseases Research Group, Department of Pharmacy, School of Health Sciences, Aristotle University of Thessaloniki, 541 24 Thessaloniki, Greece; [b]Network Center for Biomedical Research of Neurodegenerative Diseases, Institute Carlos III, Ministry of Health, 0890X L'Hospitalet de Llobregat, Spain; [c]Bellvitge Biomedical Research Institute, 08908 L'Hospitalet de Llobregat, Spain; [d]Department of Neurology, University Medical School, 37075 Göttingen, Germany; [e]Department of Genetics, Development, and Molecular Biology, School of Biology, Aristotle University of Thessaloniki, 541 24 Thessaloniki, Greece; [f]Translational Studies and Biomarkers, German Center for Neurodegenerative Diseases, 37075 Göttingen, Germany; [g]Laboratory of Pharmacology, Department of Pharmacy, School of Health Sciences, Aristotle University of Thessaloniki, 541 24 Thessaloniki, Greece; [h]Centro de Investigación en Sanidad Animal, 28130 Madrid, Spain; [i]Microarray and Deep-Sequencing Core Facility, Institute Developmental Biochemistry, University Medical Center, 37075 Göttingen, Germany; [j]Interactions Hôtes Agents Pathogenès, Institut National de la Recherche Agronomique, Ecole Nationale Vétérinaire, UMR 1225, 31300 Toulouse, France; and [k]Department of Pathology and Experimental Therapeutics, University of Barcelona, 08007 L'Hospitalet de Llobregat, Spain

Prion diseases are fatal neurodegenerative disorders caused by misfolding of the normal prion protein into an infectious cellular pathogen. Clinically characterized by rapidly progressive dementia and accounting for 85% of human prion disease cases, sporadic Creutzfeldt–Jakob disease (sCJD) is the prevalent human prion disease. Although sCJD neuropathological hallmarks are well-known, associated molecular alterations are elusive due to rapid progression and absence of preclinical stages. To investigate transcriptome alterations during disease progression, we utilized tg340-*PRNP*129MM mice infected with postmortem material from sCJD patients of the most susceptible genotype (MM1 subtype), a sCJD model that faithfully recapitulates the molecular and pathological alterations of the human disease. Here we report that transcriptomic analyses from brain cortex in the context of disease progression, reveal epitranscriptomic alterations (specifically altered RNA edited pathway profiles, eg., ER stress, lysosome) that are characteristic and possibly protective mainly for preclinical and clinical disease stages. Our results implicate regulatory epitranscriptomic mechanisms in prion disease neuropathogenesis, whereby RNA-editing targets in a humanized sCJD mouse model were confirmed in pathological human autopsy material.

prion diseases | RNA editing | sporadic Creutzfeldt–Jakob disease | RNA-sequencing | ER-stress

S poradic Creutzfeldt–Jakob disease (sCJD) is a fatal human prion disease characterized by the conversion of the cellular prion protein (PrP^C) into its pathological conformer (PrP^{Sc}), forming protein aggregates in the brain. Pathological hallmarks include gliosis, massive neuronal loss, and spongiform degeneration (1). sCJD is a heterogeneous disease, with different clinico-pathological outcomes (subtypes). sCJD sybtypes are associated with: 1) SNPs at the prion protein-coding gene (*PRNP*), especially with a SNP at codon 129 resulting in either Met or Val at the corresponding position of the protein; and 2) with PrP^{Sc} protease-resistant patterns, classified as type 1 and 2, with the latter displaying a lower molecular mass, proteinase K- (PK) resistant, immunoreactive band of unglycosylated PrP^{Sc} at 19 kDa. The most prevalent sCJD subtype (40 to 60% of all sCJD cases), designated MM1, corresponds to PrP^C methionine homozygotes displaying type 1 PrP^{Sc}. Disease manifestations include cognitive impairment, gait or limb ataxia, aphasia, mental, and visual signs, with a mean disease duration of 4 mo (2).

Prion transmission, infectivity, and mechanisms triggered by the conversion of PrP^C to PrP^{Sc} are still unknown. Advances in high-throughput transcriptomics and proteomics have identified mo-

lecular signatures associated with prion infection. Studies on in vivo prion models are crucial for disease mechanism delineation, since human disease progresses rapidly and only postmortem tissue is available. Molecular data representative of prion disease models are lacking, especially due to noncomprehensive characterization of highly related scrapie and bovine spongiform encephalopathy or other species prion diseases, by inoculation with adapted prion strains (3–6). Such diseases only partially recapitulate the molecular and neuropathological sCJD hallmarks, suggesting an urgent need for novel molecular markers describing early and later disease stages.

Significance

Prion diseases are fatal neurodegenerative disorders characterized by rapidly progressive dementia. Sporadic Creutzfeldt–Jakob disease (sCJD) is the most prevalent. We report that, specific gene-expression alterations utilizing a reliable in vivo mouse model (tg340-PRNP129MM) with sCJD MM1 subtype, correlate with human disease manifestations in the brain cortex related to disease progression. RNA-editing functions mediated by the APOBEC and ADAR deaminases possibly affecting protein expression necessary for normal brain function, are altered in disease stages. Our data provide powerful evidence, derived from a humanized sCJD mouse model and human autopsy material, discerning the critical role of gene expression and RNA-editing signatures, introducing disease-associated targets that can be extrapolated in other neurodegenerative disorders with common clinical and molecular features.

NEUROSCIENCE

We utilized a mouse model of the sCJD subtype MM1, which faithfully recapitulates human disease pathology in a regional- and subtype-dependent manner (7, 8), to investigate the regional- and temporal-dependent disease transcriptome. Transcriptomic profiles revealed regulation of both previously reported prion-associated and novel sCJD-specific related genes. We then confirmed these epitranscriptomic (RNA-editing events) findings in sCJD-affected human brain autopsy material. Our results indicate transcriptome variation, especially at preclinical disease stages of prion-induced pathology, that could clarify contributing mechanisms (i.e., lysosomal, endoplasmic reticulum stress processes) and identify potential therapeutic strategies.

Results

Differential Global Gene-Expression Analysis in the sCJD Mouse Model (tg340*PRNP*129MM). We established differential transcriptomic and epitranscriptomic profiles representative of the cortical region of sCJD tg340-*PRNP*129MM (tg340) mice at preclinical (120 d postinoculation [dpi]) and clinical (180 dpi) disease stages. Mean survival time was 199 ± 7.9 dpi, while 160 dpi was considered as an early clinical disease stage. Heat map and principle component analysis revealed clear clustering for control versus sCJD during infection (*SI Appendix*, Figs. S1 and S2). Differentially expressed (DE) were considered genes displaying a false-discovery rate (FDR)-adjusted $P \leq 0.05$ and a $\log_2$ fold-change (FC) cutoff value ≥ 0.5 (absolute value). Since any FC cutoff would be entirely arbitrary, we selected a target follow-up strategy combining the ranking of all genes based on their (absolute log) FC and the known/believed genes to be involved in the pathogenesis process. At 120 dpi 1,356 genes were identified as DE and at 180 dpi 655; 58 genes displayed deregulation toward the same direction at both time points (38 up-regulated and 20 down-regulated) (*SI Appendix*, Fig. S3). Preclinical-stage profiles involved neuronal and synaptic pathways, as well as signaling cascades associated with oxidative or endoplasmic reticulum (ER) stress. Clinical disease-stage profiles were relevant to cell survival, proliferation, differentiation, lysosome function, and immune system (*SI Appendix*, Fig. S4 and Table S1). DE profiles of prion-infected mice (RML, Me7, 22A, 79A, 139A, 22L scrapie strains) (9–15) or sCJD patients' postmortem brain tissue (16, 17) from gene-expression datasets, revealed common patterns of deregulation between our model and at least 1 of the analyzed murine prion models at preclinical and clinical disease stages (Fig. 1, *SI Appendix*, Tables S2 and S3, and Dataset S1). We detected similar profile alterations between our study and human sCJD cases. Interestingly, some genes—including *Dbi*, *Rgs4*, *Abca1*, and *Gfap*—were deregulated similarly in our study, in human sCJD cases and at least 2 scrapie-murine models (Dataset S1).

Gene-Expression Validation in the sCJD Mouse Model and in sCJD Cases. Twenty-two DE genes, novel and previously identified, were selected for qPCR validation in mouse cortical tissues (*SI Appendix*, Table S4). Comparison of the differential gene expression in sCJD and control tg340 mice with our RNA-sequencing (RNA-seq) data analysis revealed a strong correlation (R^2 and Pearson correlation coefficient [r] were $R^2 = 0.4567$ and $r = 0.6758$, $P < 0.0001$ for 120 dpi; and $R^2 = 0.5817$, $r = 0.7627$, $P < 0.0001$ for 180 dpi) (Fig. 2). Next, 14 genes—including *PRDX6*, *A2M*, *CD44*, *VIM* (Vimentin), *HMOX1*, *CD9*, *LAMP5*, *PLIN4*, *NGEF*, *SPP1*, *HSPB1* (hsp27), *DSP*, *SOCS3*, and *APOE*—were cross-validated by qPCR in human postmortem tissue with matching control samples (Fig. 3). We then validated differential protein expression of 9 proteins, including desmoplakin, c-Jun, CD44, aldehyde dehydrogenase 1 family member A1 (Aldh1a1), vimentin, insulin-like growth factor-1 (IGF1), peroxiredoxin 6 (Prxd6), heme oxygenase 1 (HMOX-1), and cystatin C in human postmortem disease with matching control samples (Fig. 4), and of desmoplakin, cathepsin D, CD44, heme oxygenase 1 (Hmox-1), clusterin, the proto-

oncogene c-Jun, Aldh1a1, vimentin, and Prxd6, in sCJD and control tg340 mice (Fig. 5). As negative control, we analyzed the levels of early growth response 1 (EGR-1), which was found exclusively regulated at preclinical stages in the sCJD mouse model, and accordingly its expression levels were not altered in sCJD postportem tissue (Fig. 4).

Editing Analysis in the sCJD Mouse Model (tg340*PRNP*129MM). RNA editing and correlation of editing events in the brain with neurodegenerative (ND) and neurological diseases (18–21), suggest differences in global ADAR and APOBEC editome profiles between control and sCJD animals. We determined global RNA-editing profiles (editomes) in control and sCJD mice at different disease stages using an in-house pipeline (*SI Appendix*, Fig. S5; editome profile lists are provided in Dataset S2; diagrammatic representation of RNA editomes per animal group and time-point is shown in *SI Appendix*, Fig. S6). DNA–RNA differences and the number of events for the 12 types of differences between RNA reads and genomic DNA sequences showed that putative editing is highly concordant between biological replicates. Strikingly, over 90% of these sites correspond to A-to-G and C-to-T differences, consistent with A-to-I and C-to-U editing. This observation supports the existing knowledge that A-to-I editing is the primary type of RNA editing. Other types of differences are much less abundant. ADAR-mediated editing is predominant in the mouse cortex compared to APOBEC-mediated editing (*SI Appendix*, Fig. S6, ring A). Similar genomic distributions of editing events were observed for all tested groups and time-points. Most editing events were detected in intergenic regions, 3′UTRs, exons, or introns, while fewer were in 5′UTRs and other noncoding regions (*SI Appendix*, Fig. S6, rings B and C). Profiling of control and sCJD animals' editomes for each time point and clinical stage revealed high similarities between the 2 animal groups and only a few transcripts were uniquely edited either in control or in sCJD. In contrast to global editomes, differentially edited transcript analysis showed APOBEC-mediated editing is overrepresented (~49 to 60%) (Dataset S3) in almost all phenotypic groups and time points (Fig. 6, ring A). Dissimilar genomic distributions highlight an increase of 3′UTR editing events in sCJD animals compared to controls at clinical disease (Fig. 6, rings B and C). The observed increase in 3′UTR editing is mainly attributed to APOBEC, even though A-to-I editing is also increased at this stage. Differentially edited transcripts at clinical disease displayed alterations in other noncoding regions, while few edited exons (~5%) were detected among the differentially edited transcripts at this time point. At preclinical disease stage, a clear preference of ADARs to edit intronic and 3′UTR regions was observed, while APOBEC editing was mostly detected in exonic and intergenic regions (Fig. 6, rings B and C). Only a few edited transcripts were unique either in control (30% in preclinical and 27% at clinical stage) or in sCJD animals (28% at preclinical and 11% at clinical disease).

Gene ontology (GO) and pathway analyses of the differential editomes at preclinical and clinical disease stages revealed dendrite-associated transcripts involved in cell adhesion and junction signaling at preclinical disease. At clinical disease, immune related transcripts were significantly represented, but no pathway was significantly enriched.

RNA Editing Validation in the sCJD Mouse Model and in sCJD Cases. Uniquely edited transcripts in each group, or edited at the same position at both groups yet at differential editing rates, were validated as a proof-of-concept to our in silico RNA editing profiling. These included *Fkrp*, *Plekhm2*, and *Sidt2* (preclinical), as well as *Sec61a1* and *Rragd* (clinical) in mice (Table 1 and *SI Appendix*, Figs. S7 and S8). Next, we cross-validated differentially edited mouse targets in human postmortem tissue, including 2 APOBEC (*PAQR8*, *B2M*) and 2 ADAR targets (*CTSS*, *RRAGD*) (Table 1). Sequencing analysis of PCR products or adequate number of
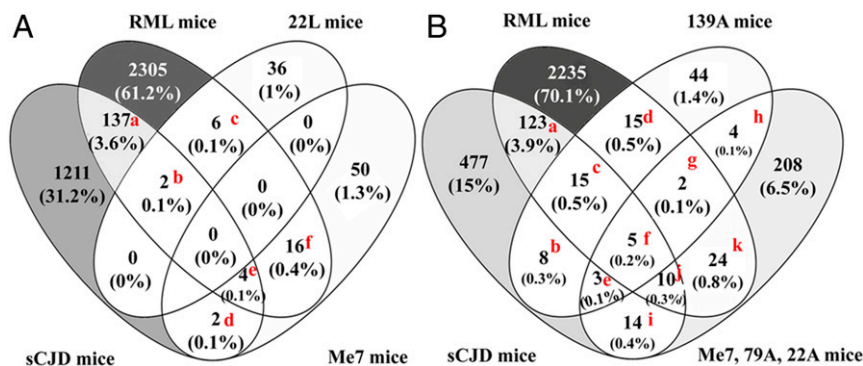
Fig. 1. Correlation of sCJD-mice gene-expression alterations at preclinical and clinical disease stages with corresponding alterations determined in scrapie-murine models. Venn diagrams displaying the overlap of gene-expression alterations at preclinical (*A*) and clinical (*B*) stages among different models of prion diseases. Significant overlaps are observed between sCJD-mice and the tested scrapie models. For a complete list of overlapping genes, please refer to *SI Appendix*, Tables S2 and S3 and Dataset S1.

clones harboring the transcript regions under study and comparison with the corresponding genomic reference sequence, confirmed the presence of differential editing between control and sCJD animals for most of the tested targets (Table 1 and *SI Appendix*, Figs. S7 and S8). We confirmed APOBEC differential editing at the preclinical disease stage in *Fkrp* and *Sidt2* transcripts; *Fkrp* displays editing of C at position Chr7:16809815 (relative to the mm10 reference genome) only in the disease group (*SI Appendix*, Fig. S7). Furthermore, C editing at position Chr9:45941373 in the *Sidt2* transcript is significantly reduced in sCJD animals compared to controls. *Sidt2* also undergoes ADAR-mediated editing in A at positions Chr9:45939224 and Chr9:45939169, and similarly to APOBEC editing, displays reduced editing rates in the diseased animals (*SI Appendix*, Fig. S8). At the clinical disease stage, we identified differential A-to-I editing in the murine *Rragd* 3′UTR (Chr4:33020417), showing increased editing levels in sCJD-tg340 animals (*SI Appendix*, Fig. S8).

In human samples, we identified APOBEC-catalyzed RNA–DNA sequence differences (RDDs) in the human *PAQR8* 3′ UTR (Chr6:52406406, coordinate given relative to hg38), presenting higher editing in control samples (Table 1 and *SI Appendix*, Fig. S9). Additionally, we identified a C-to-U editing event in the sCJD *B2M* transcript (Chr15: 44713183), at a frequency of 10% (3 of 30 tested clones). The same *B2M* position appears as "pre-edited" at the genomic DNA (gDNA) level of the tested control sample (Table 1 and *SI Appendix*, Fig. S9). Furthermore, we identified increased A-to-I editing in the 3′UTRs of human *CTSS* (significantly different sites at positions Chr1:150731266, Chr1:150731240, Chr1:150731200, Chr1:150731196, Chr1:150731185, Chr1:150731144, Chr1:150731143, Chr1:150731137, Chr1:150731136) (see also Table 1 and *SI Appendix*, Figs. S10–S12) and *RRAGD* (significantly different sites at positions Chr6:89366492, Chr6:89366490, Chr6:89366416, Chr6:89366335, Chr6:89366271) transcripts in sCJD cases postmortem brain tissue compared to control samples (Table 1 and *SI Appendix*, Fig. S12).

Discussion

Utilizing a humanized sCJD mouse model, recapitulating faithfully human disease, we studied preclinical and clinical disease stages. We used RNA-seq analysis to identify transcriptome and RNA editome alterations during disease progression. DE genes at both preclinical and clinical disease stages included previously identified and similarly deregulated genes in different scrapie-infected mice. Comparison of our sCJD mice data with human sCJD case transcriptomic data identified 19 commonly regulated genes, including *Abca1*, *Capg*, *Car10*, *Cst3*, *Dbi*, *Dhcr24*, *Diras2*, *Gabrd*, *Gfap*, *Itpkb*, *Itpr1*, *Lrig1*, *Mt1*, *Npc2*, *Pcp4*, *Rab31*, *Rgs4*, *Rin2*, and *Tnfrsf1a*, indicating a common expression profile between the utilized sCJD

mouse model and human sCJD. Furthermore, commonly deregulated genes were identified between sCJD mice, human sCJD cases, and scrapie murine models, suggesting significant overlap regarding gene-expression perturbations triggered by different strains of animal (scrapie) and human (sCJD) diseases. Remarkably, *Abca1*, *Dbi*, *Gfap*, and *Rgs4* presented common deregulation patterns among sCJD mice, human sCJD cases (16, 17), RML mice (9), and Me7/79A/22A mice (14). Collectively, we suggest that different prion strains induce both common and differential responses to their hosts, with the highest variability being associated with preclinical disease stages. Corroborating the notion that common and variable gene-network profiles are induced by different strains at preclinical disease, temporal differences correlating with the pace of infection have been identified regarding the inflammatory responses triggered by strain-specific brain PrP^{Sc} accumulation in the thalamus of affected animals (22). Early PrP^{Sc} accumulation is believed to induce pathogenetic mechanisms, as well as cellular responses aiming at induction of countervailing cellular responses, which fail to restore cellular homeostasis, resulting in disease progression. Majer et al. (10) reported the induction of cell survival and neurite remodeling pathways in hippocampal neurons of RML-infected mice at preclinical disease and suggested asymptomatic disease as a critical time point for intervention. In contrast, clinical disease-related molecular mechanisms, when extensive degeneration has been established, are
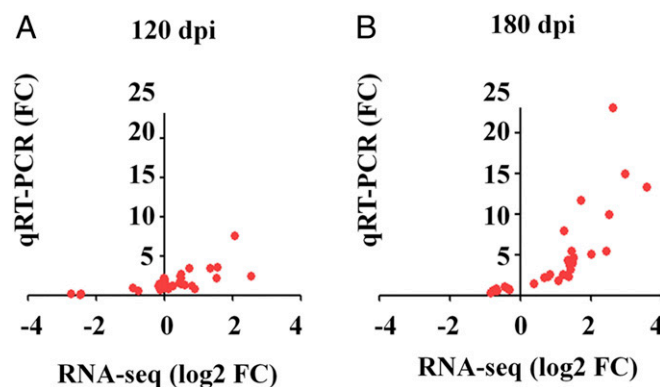
Fig. 2. Correlation of RNA-seq data with RT-qPCR experimental validations in sCJD (tg340) mice. Correlation of gene-expression values between RNA-seq and RT-qPCR. R^2 and Pearson correlation coefficients (*r*) for each time point were as follows: (*A*) 120 dpi: $R^2 = 0.4567$, $r = 0.6758$; (*B*) 180 dpi: $R^2 = 0.5817$, $r = 0.7627$. Statistically significant correlation between in silico and experimental analyses was detected for both time points (***$P < 0.0001$).

Fig. 3. Experimental cross-validation of RNA-seq data in postmortem sCJD MM1 subtype cases by RT-qPCR. RNAs from control (n = 12) and postmortem sCJD patients of the MM1 subtype (frontal cortex region n = 8) were retrotranscribed and tested using Taqman probes to determine human gene expression; human genes were selected based on the corresponding analysis in the sCJD (tg340) mouse model (clinical disease, 1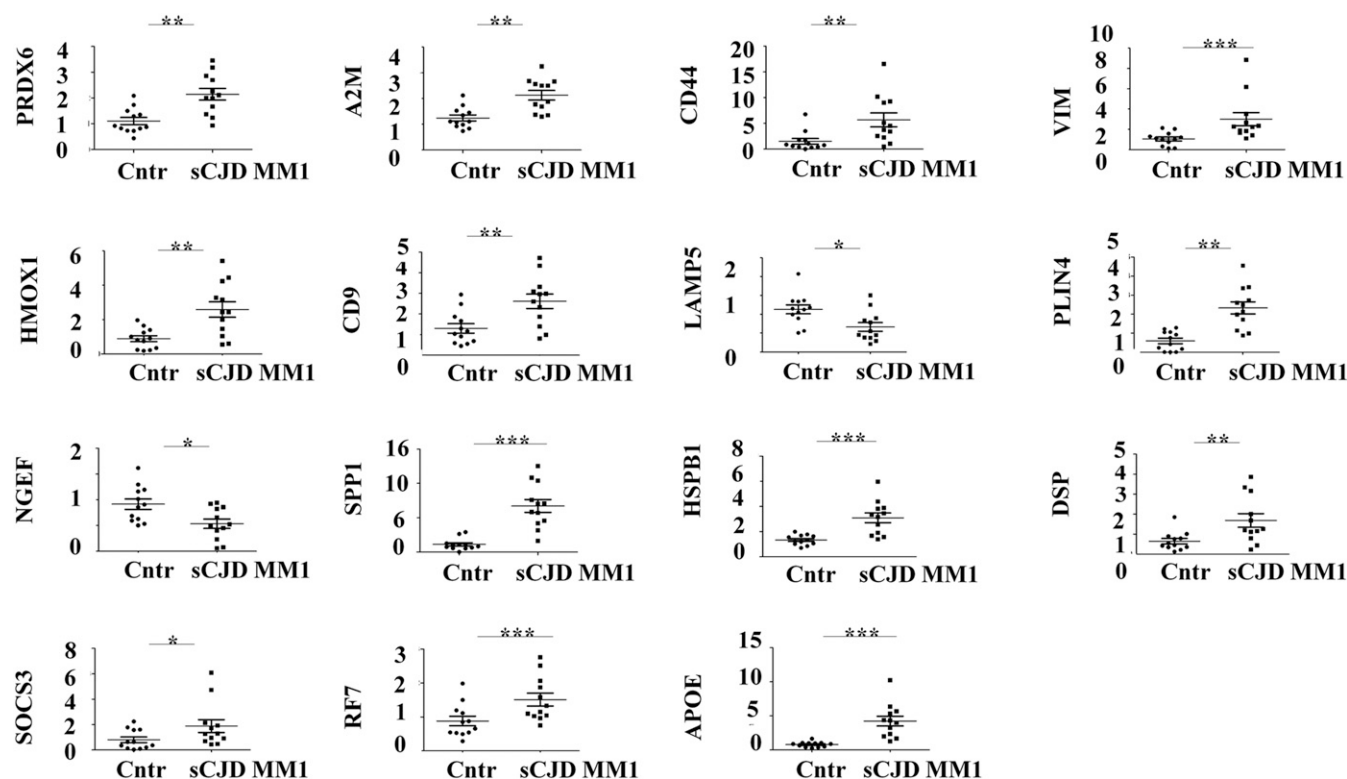80 dpi). *GAPDH* was used for normalization. Following a D'Agostino and Pearson test to verify the normality of the distribution, mean FC values were compared in disease and control cases using the Mann–Whitney U test. *P < 0.05, **P < 0.01, and ***P < 0.001.

more likely to reflect infection. We provide proof-of-principle experimental validations of prion disease-specific transcriptomic profiles at the mRNA and protein level using murine and human sCJD autopsy material. Twenty of 34 DE-validated targets were previously associated with prion diseases, and 14 novel ones are being disease-associated herein (*SI Appendix*, Table S5). Of notice are: PRDX6, found to attenuate prion-related neuropathology in *Prdx6* knockout mice infected with the Me7 scrapie strain (23); TREM2, involved in microglia activation upon prion infection (24); cathepsin D (*Ctsd*), reported to prevent a-synuclein aggregation and toxicity in in vivo models of Parkinson's disease (25); and cystatin C (*Cts3*), found to inhibit Aβ oligomerization in both in vivo Alzheimer's disease models and in in vitro studies (26), supporting similar mechanisms on PrP^Sc aggregates in prion diseases. Additionally, we introduced the validated contribution of the epigenetic mechanism of RNA editing in disease-associated molecular targets. Triggered by the highly unknown etiology of sCJD and by reports on the effects of RNA-editing perturbations in neoplastic disease (27–31) and more importantly in neurological and ND disorders (19, 32–34), we established differential editome profiles in the cortex of control and sCJD animals, at preclinical and clinical disease stages, based on an in-house bioinformatics pipeline with stringent criteria to exclude false-positive single-nucleotide variants. To limit false-positive in silico RNA-editing identification and increase the validity of our analysis, we have introduced multiple algorithms and filtering steps in addition to well-accepted in the field quality control analyses, including the assessment of whole RDD mismatch spectrum representation and estimation of editing event enrichment in repetitive regions. Furthermore, we searched for potential pseudogenes among the targets detected to undergo RNA editing, which ruled out the

possibility of detecting false-positive RNA-editing events due to duplications. We and others describe ADAR-mediated editing as prevalent in the mouse cortex (>50% of total editing events) (32, 35) and identify a significant representation of C-to-U RDDs occurring as a result of APOBECs' catalytic action. This places our study among those reporting significant APOBEC-mediated RNA editing in murine brain, including only 1 recent study by Cole et al. (36), which has investigated RNA editing in mouse brain microglia, while other previous APOBEC-induced RNA-editing studies focused on other mouse tissues, in particular small intestine, liver (37, 38), and macrophages (39). The validity of our approach is highlighted by the overlap between our results and previously reported editing sites in similar tissues. Several editing events identified here have been reported in mice, including conserved editing events in the mammalian brain and experimentally validated alterations in murine tissues (*SI Appendix*, Table S6).

Five sites, residing in the 3′UTR of *B2m* (chr2: 122152682, chr2: 122152902), *Cisd2* (chr3: 135406870), *Rragd* (chr3: 33020417), and downstream of *Smim14* (chr5: 65448046) displayed similar editing-rate alterations between our sCJD and an epilepsy mouse model (32). Differential editing characterized by reverse-frequency alterations between these 2 models was observed at the 3′UTR of the *Nt5dc3* (chr10: 86837257), *Ankrd28* (chr14: 31700662), and *Gpm6b* (chrX: 166387925) transcripts, as well as in *Gria2* exon 11 (chr3: 80706908, synonymous change); the latter is also differentially edited in Alzheimer's disease patients (19).

Our data identified reduced differential editing with disease progression. Gene expression and protein level analysis of the main RNA-editing enzymes in mouse (ADAR1, ADAR2, APOBEC1, and APOBEC3) did not reveal any significant changes during disease progression between control and sCJD animals, with the
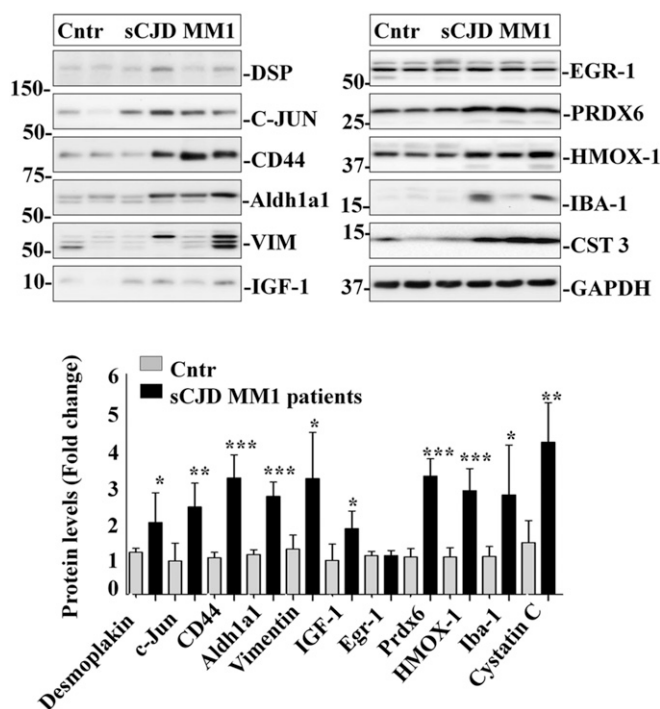
Fig. 4. Experimental cross-validation of RNA-seq data in postmortem sCJD MM1 subtype cases by Western blot. Western blot analysis of Desmoplakin, c-Jun, CD44, Aldh1a1, vimentin, IGF1, EGR-1, PRDX6, HMOX-1, IBA-1, and cystatin C in sCJD patient postmortem brain tissue. GAPDH was used as loading control. Densitometries derived from the quantification of 6 cases per group are shown. Following a D'Agostino and Pearson test to verify the normality of the distribution, mean FC values were compared in disease and control cases using the Mann–Whitney U test. *$P < 0.05$, **$P < 0.01$, and ***$P < 0.001$.

exception of decreased ADAR2 mRNA expression in affected animals at clinical disease ($P = 0.0231$). Similarly, reduced ADAR2 protein expression was observed without reaching statistical significance ($P = 0.5183$). Our data are in agreement with Srivastava et al. (32), who also reported reduced ADAR2 expression in epileptic mice. This finding correlates with the observed RNA-editing reduction during disease progression reported in our study, even though additional factors possibly affecting ADAR2 access to targeted RNAs may contribute to the observed difference.

The finding that global RNA editing is reduced during disease progression enhances our strategy to focus on preclinical RNA-editing perturbations for delineating driver disease events and identifying novel potentially therapeutic targets. We identified the cAMP signaling pathway and neuronal transcripts as enriched in differentially edited transcripts at the preclinical disease stage, additionally supported by previous studies reporting synaptic dysfunction as an early event in prion pathogenesis (40, 41). Further studies could focus on differentially edited transcripts, such as *Gria2*, *Gria4*, *Pde4d* (involved in synaptic plasticity), and *Sidt2* [implicated in lysosome and or Golgi related processes, all of which are impaired in prion diseases (42–48)]. We have identified individual RNA-editing events in clinical disease stage, supporting the notion that they could represent key molecular disease triggers, even though significantly enriched pathways were not observed. Differentially edited transcripts, including the microglia enriched and immune related *B2m*, as well as ER-related transcripts (49), such as *Sez6l2* (50) and *Sec61a1* (51), could represent candidate targets for future functional RNA-editing validation studies.

Regarding RNA-editing analyses in human autopsy samples, we cross-validated differentially edited targets (*CTSS*, *RRAGD*) identified from the analysis of the utilized mouse model; furthermore, we used a small cohort of RNA samples for expression analysis at the gene level ($n = 5$ control, $n = 3$ sCJD) and valuable brain homogenates for expression analysis at the protein level ($n = 4$ control, $n = 4$ sCJD), in order to determine the expression levels of the main RNA-mediating enzymes in humans, namely ADAR1, ADAR2, APOBEC1, and APOBEC3G. We did not detect significant differences in the expression levels of these key editing enzymes between sCJD and control samples, with the exception of ADAR2, which could not be detected at the protein level in the control samples. This result seems to be in contrast to the corresponding analysis of the utilized murine model, possibly suggesting differences regarding the main editing enzyme expression levels between our model and human disease. Even though we cannot exclude the possibility of the occurrence of such differences, we should interpret these data by taking into account the rarity of available samples and the variability in their processing and storage.

The human cross-validated RNA-editing targets have been reported by others as possible contributors to ND disease pathogenesis. Specifically, cathepsins and particularly *CTSS* have been implicated in prion disease pathogenesis (8), as well as in other NDs (52), including multiple sclerosis (53) and Alzheimer's disease (54). Additionally, *RRAGD* is involved in amino acid signaling induced mammalian target of rapamycin (mTRORC1) pathway activation (55); mTORC1 controls organism growth through
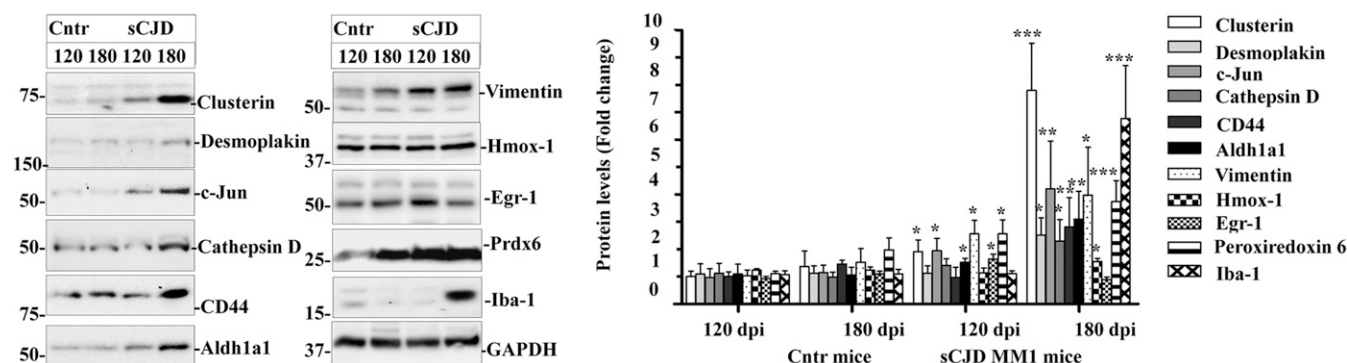

Fig. 5. Experimental validation of RNA-seq data in sCJD (tg340) mice at protein level. Western blot analysis of clusterin, desmoplakin, c-Jun, cathepsin D, CD44, Aldh1a1, vimentin, Hmox-1, Egr-1, Prdx6, and Iba-1 at preclinical (120 dpi) at clinical (180 dpi) disease stages in the tg340 mice inoculated with brain homogenates from control and postmortem sCJD cases of the MM1 disease subtype. Following a D'Agostino and Pearson test to verify the normality of the distribution, mean FC values were compared between diseased and control animals for each time point using the Mann–Whitney U test. GAPDH was used as a loading control protein. Densitometries derived from the quantification of 3 animals per group are shown. *$P < 0.05$, **$P < 0.01$, and ***$P < 0.001$.
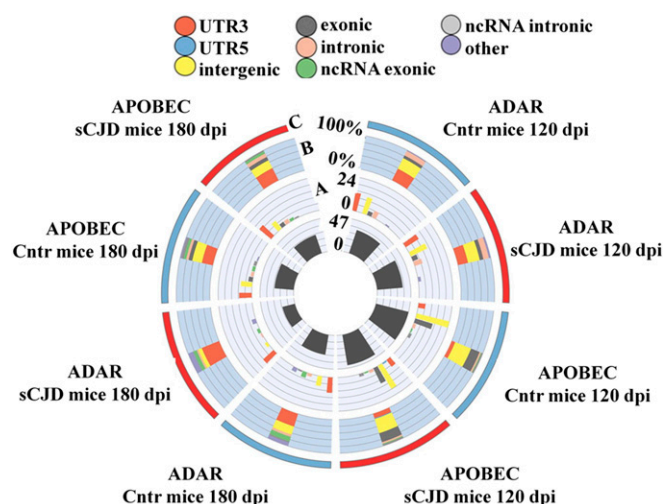
Kanata et al.

Fig. 6. Differential editing profiles of control and sCJD-tg340 mice at preclinical and clinical disease stages. Differential editing was identified as indicated in the text. Ring A: Bars indicate the absolute number of RNA editing sites displaying differential editing for each phenotype (cntr, sCJD), RNA-editing mediating enzyme (ADAR, APOBEC), and disease time point (preclinical: 120 dpi, clinical: 180 dpi). Ring B: Genomic distribution (color code legend on top of the graph) of differential editing events for each phenotype, RNA-editing mediating enzyme and disease time point. The bars indicate the absolute number of positions identified. Ring C: Percent genomic distribution (color code legend on top of the graph) of differential editing events for each phenotype, RNA-editing mediating enzyme and disease time-point. The bars visualize the distribution of RNA-editing positions across functional gene regions calculated as a percentage of the total RNA-editing positions identified in each phenotype. For a detailed list of differentially editing events between the studied animal groups and time points, refer to Dataset S3.

regulation of cellular processes, including autophagy and lysosome biogenesis, and is deregulated in NDs. *RRAGD* participates in endosome/lysosome biogenesis and thus in cellular clearance, suggesting that differential editing in this target is associated with disease pathogenetic mechanisms referring to cellular clearance processes (56). Finally, the *PAQR8* transcript, validated as differentially edited in human sCJD autopsy brain tissue, encodes a member of the adipoQ progesterone receptor family and has been associated with epilepsy (57), suggesting that its aberrant forms could be involved in other brain disorders, including prion diseases. Functional importance of the newly identified and validated targets in human tissue is highlighted by the predicted changes in microRNA binding sites with probable effects on the altered gene expression of the mRNA targets (*CTSS*, *RRAGD*, *PAQR8*) (*SI Appendix*, Fig. S13).

Our study utilized a faithful sCJD murine model to identify disease progression transcriptomic profiles and corresponding epitranscriptomic (RNA editing) signatures in human autopsy material. Taking into account that RNA editing displays species-specific differences and keeping in mind potential limitations of the murine model utilized in this study regarding human disease aspects representation, we provide experimental evidences that provide proof-of-principle validations of novel disease-associated targets in human.

Materials and Methods

Antibodies. Anticathepsin D, anti–c-Jun, and anti–Egr-1 were from Santa Cruz; anti–Iba-1 was from Wako; anti-CD44 was from Cell Signaling; antivimentin was from Dako; anti-GAPDH, antidesmoplakin, anti–HMOX-1, anti-Prdx6, anti-ALDH1A1, and anti- IGF1 were from Abcam; antiheat-shock protein 27 (hsp27) was from Novus; anticlusterin was from Chemicon, anticystatin C was from Upstate; and anti-α-actin was from Sigma.

Human Cases. Brain tissue was obtained from the Institute of Neuropathology Brain Bank (HUB-ICO-IDIBELL Biobank) following pertinent guidelines of local ethics committees. All procedures involving human participants were in accordance to the 1964 Helsinki declaration and its later amendments or comparable ethical standards. Neuropathological examination and characterization was carried out in every case on paraffin-embedded samples. Detailed neuropathology, inflammatory profiling, and demographics of the cohort is described elsewhere (58, 59). Control samples did not present any infectious, metabolic, or neoplastic disease. No correlation between postmortem delay or sample storage time and levels of analyzed proteins and mRNA were observed. Age- and gender-matched cases were used. For qPCR analysis, 12 control samples ($n = 12$, 6 males/6 females) corresponding to individuals of mean age 65 ± 9 y and 12 postmortem sCJD samples ($n = 12$, 7 males/5 females) from patients of the MM1 disease subtype with mean age 66 ± 8 y were used. For Western blot analysis, 6 controls ($n = 6$, 3 males/3 females, mean age 63 ± 11 y) and 6 postmortem sCJD MM1 ($n = 6$, 4 males/2 females, mean age 65 ± 9 y) samples were analyzed.

sCJD Mice Model–tg340-*PRNP*129MM The tg340 mouse line expressing about 4-fold level of human PrP MM129 (Met at codon 129) on a mouse PrP-null background was generated as described previously (60). Control or postmortem brain tissues (10% [wt/vol] homogenates) from the MM1 subtype of a sCJD patient were inoculated in 6- to 10-wk-old mice in the right parietal lobe, using a 25-gauge disposable hypodermic needle. Mice were observed daily and their neurological status was assessed weekly. Animals were killed at presymptomatic (120 dpi) and symptomatic (180 dpi) stages. Survival time was calculated and expressed as the mean of the survival day postinoculation of all mice scoring positive for PrP^{Sc}. Infection rate was determined as the proportion of mice scoring positive for PrP^{Sc} from all inoculated mice. All animal experiments were performed in compliance with the French national guidelines, in accordance with the European Community Council Directive 86/609/EEC. Experimental protocol was approved by the Institut National de la Recherche Agronomique Toulouse/École Nationale Vétérinaire de Toulouse ethics committee. For RNA-seq and qPCR analysis, 4 animals per group and time point were used; for immunoblotting, samples from 3 to 4 animals per group and time point were analyzed.

RNA Purification. RNA was purified using the miRVANA RNA isolation kit, following the manufacturer's protocol. RNAs were treated with DNase Set (Qiagen) for 15 min to eliminate genomic DNA contamination. RNA integrity was assessed by its corresponding RNA Integrity Number (RIN value), determined with the Agilent 2100 Bioanalyzer (Agilent).

RNA-Seq and Differential Gene-Expression Analysis. Libraries were prepared using the TruSeq RNA Sample Preparation v2 kit (Illumina). Library quality was assessed with an Agilent 2100 Bioanalyzer and a Qubit dsDNA HS Assay Kit. RNA sequencing was performed as described in ref. 61. All original RNA-seq data were deposited in the National Center for Biotechnology Information's Gene Expression Omnibus, GEO accession no. GSE90977. Briefly, RNA-seq data were subjected to an in-house quality control workflow. Read quality was assessed using FastQC (v0.10.1), to identify sequencing cycles with low average quality, adapter contamination, or repetitive sequences from PCR amplification. Alignment quality was analyzed using SAMtools flagstat (v0.1.18), with default parameters. Sequences were aligned to the genome using gapped alignment, as RNA transcripts are subject to splicing and reads might therefore span 2 distant exons. Reads were aligned to the whole *Mus musculus* mm10 genome using STAR aligner (62) (2.3.0e_r291) with default options, generating mapping files (BAM format). Read counts for all genes and all exons (Ensembl annotation v72) were obtained using FeaturesCount (http://bioinf.wehi.edu.au/featureCounts/). For data visualization, BAM files were converted into WIG and BigWig files using the MEDIPS "MEDIPS.exportWIG" function with a window of 50 bp and RPM normalization. For the differential expression analysis, read counts generated with FeaturesCount were compared between groups using DESeq2 (63). Genes with a $\geq 0.5 \log_2$ FC cutoff and FDR-adjusted $P \leq$ to 0.05 were considered as differentially expressed.

Differential Gene-Expression Validations.
Real-time qPCR (RT-qPCR). RNA samples were reverse transcribed using the High Capacity cDNA Archive kit (Applied Biosystems). qPCR assays were performed in duplicate on cDNA samples in a LightCycler 480 System (Roche). Reactions were set up using 20 × TaqMan Gene Expression Assays (*SI Appendix*, Table S7) and 2xTaqMan Universal PCR Master Mix (Applied Biosystems). The FC was determined using the equation $2^{-\Delta\Delta CT}$. Mean FC values were analyzed with appropriate statistical tests, indicated in the corresponding figures, using GraphPad Prism 6.01.

Table 1. Summary of potential disease-associated RNA editing events that have been experimentally verified in the tg340-sCJD mouse model and in human sCJD cases in this study

Species	Condition	Time point (dpi)*	Target	Coordinates†	Nt Ref/change	Editing detection/frequency (Rel. or %)‡
M	Cntr	**120**	***Fkrp***	**Chr7:16809815**	C/T	No/0§,¶
M	sCJD	120	*Fkrp*	Chr7:16809815	C/T	Yes/High§,¶
M	Cntr	120	***Plekhm2***	**Chr4:141626449**	C/T	Yes/Medium§,#
M	sCJD	120	*Plekhm2*	Chr4:141626449	C/T	No/0§,#
M	Cntr	120	***Sidt2***	**Chr9: 45941373**	C/T	Yes/84¶,‡‡,**
M	sCJD	120	*Sidt2*	Chr9: 45941373	C/T	Yes/48¶,‡‡,**
M	Cntr	120	***Sidt2***	**Chr9:45939224**	A/G	Yes/96¶,‡‡,**
M	sCJD	120	*Sidt2*	Chr9:45939224	A/G	Yes/48¶,‡‡,**
M	Cntr	120	***Sidt2***	**Chr9:45939169**	A/G	Yes/96¶,‡‡,**
M	sCJD	120	*Sidt2*	Chr9:45939169	A/G	Yes/48¶,‡‡,**
M	Cntr	180	***Sec61a1***	**Chr6:88504590**	C/T	Yes/High§,#
M	sCJD	180	*Sec61a1*	Chr6:88504590	C/T	No/0§,#
M	Cntr	180	***Rragd***	**Chr4: 33020417**	A/G	Yes/30¶,∥,**
M	sCJD	180	*Rragd*	Chr4: 33020417	A/G	Yes/74¶,∥,**
H	Cntr	180	***PAQR8***	**Chr6: 52406406**	C/T	Yes/43††
H	sCJD	180	*PAQR8*	Chr6: 52406406	C/T	No/0††
H	Cntr	180	***B2M***	**Chr15: 44713183**	T/T	NA††
H	sCJD	180	*B2M*	Chr15: 44713183	C/T	Yes/10††
H	Cntr	180	***CTSS***	**Chr1:150731266**	A/G	No/0‡‡,§§,¶¶,##
H	sCJD	180	*CTSS*	Chr1:150731266	A/G	Yes/10‡‡,§§,¶¶,##
H	Cntr	180	***CTSS***	**Chr1:150731240**	A/G	No/0‡‡,§§,¶¶,##
H	sCJD	180	*CTSS*	Chr1:150731240	A/G	Yes/15‡‡,§§,¶¶,##
H	Cntr	180	***CTSS***	**Chr1:150731200**	A/G	Yes/15‡‡,§§,¶¶,##
H	sCJD	180	*CTSS*	Chr1:150731200	A/G	Yes/50‡‡,§§,¶¶,##
H	Cntr	180	***CTSS***	**Chr1:150731196**	A/G	Yes/7‡‡,§§,¶¶,##
H	sCJD	180	*CTSS*	Chr1:150731196	A/G	Yes/34‡‡,§§,¶¶,##
H	Cntr	180	***CTSS***	**Chr1:150731185**	A/G	Yes/7‡‡,§§,¶¶,##
H	sCJD	180	*CTSS*	Chr1:150731185	A/G	Yes/22‡‡,§§,¶¶,##
H	Cntr	180	***CTSS***	**Chr1:150731144**	A/G	No/0‡‡,§§,¶¶,##
H	sCJD	180	*CTSS*	Chr1:150731144	A/G	Yes/9‡‡,§§,¶¶,##
H	Cntr	180	***CTSS***	**Chr1:150731143**	A/G	No/0‡‡,§§,¶¶,##
H	sCJD	180	*CTSS*	Chr1:150731143	A/G	Yes/20‡‡,§§,¶¶,##
H	Cntr	180	***CTSS***	**Chr1:150731137**	A/G	No/0‡‡,§§,¶¶,##
H	sCJD	180	*CTSS*	Chr1:150731137	A/G	Yes/56‡‡,§§,¶¶,##
H	Cntr	180	***CTSS***	**Chr1:150731136**	A/G	No/0 ‡‡,§§,¶¶,##
H	sCJD	180	*CTSS*	Chr1:150731136	A/G	Yes/31‡‡,§§,¶¶,##
H	Cntr	180	***RRAGD***	**Chr6:89366492**	A/G	No/0‡‡,##
H	sCJD	180	*RRAGD*	Chr6:89366492	A/G	Yes/7‡‡,##
H	Cntr	180	***RRAGD***	**Chr6:89366490**	A/G	No/0‡‡,##
H	sCJD	180	*RRAGD*	Chr6:89366490	A/G	Yes/7‡‡,##
H	Cntr	180	***RRAGD***	**Chr6:89366416**	A/G	Yes/1‡‡,##
H	sCJD	180	*RRAGD*	Chr6:89366416	A/G	Yes/23‡‡,##
H	Cntr	180	***RRAGD***	**Chr6:89366335**	A/G	Yes/3‡‡,##
H	sCJD	180	*RRAGD*	Chr6:89366335	A/G	Yes/20‡‡,##
H	Cntr	180	***RRAGD***	**Chr6:89366271**	A/G	No/0‡‡,##
H	sCJD	180	*RRAGD*	Chr6:89366271	A/G	Yes/5‡‡,##

Entries presented in bold font represent different RNA editing events that have been detected in the present study. Cntr, control; H, human; M, mouse; NA, not applied; sCJD, sporadic CJD.

*"120 dpi" refers to preclinical and "180 dpi" refers to clinical diseases stage in the tg340-sCJD mouse model. Human samples refer to end-point disease.

†Coordinates given relative to mm10 *Mus musculus* genome for murine targets and relative to GRCh38 for human targets.

‡Relative editing frequency determined as low, medium, or high based on analysis of PCR amplified cDNA samples (in cases where our in silico analysis identified editing events as unique in either the control or in the sCJD group). Editing frequency estimated based on analysis of cDNA clones (in cases where our in silico analysis identified editing events in both control and sCJD groups, yet at different frequencies).

§Experimental validation refers to Sanger sequencing analysis of cDNA amplified products corresponding to 3 animals of the same phenotype group. Representative chromatograms of these experimental validations are provided in *SI Appendix*, Fig. S7.

¶gDNA analysis of littermates of the tested animal groups (>10 per group) did not reveal any gDNA variation at the corresponding position.

#gDNA analysis of littermates of the tested animal groups (>10 per group) identified genetic variation at the corresponding position.

∥Experimental validation refers to Sanger sequencing analysis of adequate cDNA clones (~20) corresponding to 1 animal per phenotype group.

**Representative chromatograms and clone alignments of these experimental validations are provided in *SI Appendix*, Fig. S8.

††Experimental validation refers to Sanger sequencing analysis of adequate cDNA clones corresponding to 1 control and 1 sCJD case. Representative chromatograms and clone alignments of these experimental validations are provided in *SI Appendix*, Fig. S9.

‡‡Experimental validation refers to Sanger sequencing analysis of adequate cDNA clones corresponding to 3 control and 3 sCJD cases.

§§Representative alignments of the hu-*CTSS* 3′UTR for 1 control and 1 sCJD sample are shown in *SI Appendix*, Fig. S10.

¶¶Summary of hu-*CTSS* 3′UTR alignments including the statistically significant differentially edited positions across all 3 tested samples per group are shown in *SI Appendix*, Fig. S11.

##Diagrammatic representation of the statistically significant differentially edited positions in human *CTSS* and *RRAGD* 3′UTRs is provided in *SI Appendix*, Fig. S12.

Immunoblotting. Human and mice tissues were lysed in Lysis Buffer containing 100 mM Tris pH 7, 100 mM NaCl, 10 mM EDTA, 0.5% Nonidet P-40 and 0.5% sodium deoxycolate plus protease and phosphatase inhibitors. After centrifugation at $14.000 \times g$ for 20 min at 4 °C, supernatants were quantified for protein concentration (Bradford, Bio-Rad), mixed with SDS/PAGE sample buffer, boiled, and subjected to 8 to 15% SDS/PAGE. Gels were transferred onto PVDF membranes and processed for specific immunodetection using an electrochemiluminescence reagent. For Western blot comparative analysis 10 human cases and 3 mice samples per condition were analyzed.

Statistical Analysis. For qPCR and Western blot experiments, normality distribution was analyzed following the D'Agostino and Pearson test. Mann–Whitney U tests were used to compare 2 groups of samples. GraphPad Prism 6.01 was used for statistical calculations. Differences between groups were considered statistically significant at *$P < 0.05$, **$P < 0.01$, and ***$P < 0.001$.

Bioinformatics Pipelines for Identification of RNA Editing Events.
Quality control and processing of RNA-seq raw data. High-depth RNA-seq data (26 to 58 million reads per sample, average 33 million reads per sample, GEO accession no. GSE90977) were subjected to quality control analyses using the FastQC software. Adapter sequences, as well as the first 6 bases of the 5′ end and the first 3 bases of the 3′ end of each read were trimmed utilizing the Trim Galore software (http://www.bioinformatics.babraham.ac.uk/projects/trim_galore/). Adapter sequence contamination was removed and false-positive RNA editing calls originating from random hexamer primer bias were minimized (64, 65), trimming excluded reads displaying lengths lower than 20 bases. Processed reads were aligned against the mouse reference genome (mm10), using TopHat2 software (66) (https://ccb.jhu.edu/software/tophat/index.shtml). Higher mapping rates were allowed by providing a set of known gene annotations for the reference mm10 genome. Multimapping reads were excluded and up to 3 mismatches per read were allowed. A high proportion of acquired reads (98.7 to 99%, average 98.8%) were mapped to the murine reference sequence. Pertinent data for each of the analyzed samples is provided in *SI Appendix*, Table S8. Calling of single-nucleotide variants for the identification of possible RNA-editing events was performed utilizing 2 approaches based on the REDItools (67) and VarScan (68) suites, respectively. For the REDItools suite, an initial Blat Correction analysis (using the script REDItoolBlatCorrection.py) was performed to identify ambiguous aligning reads and the REDItoolDenovo.py script was subsequently used to call possible RNA editing events. For the VarScan suite, the function mpileup2snp was used to process pile-up files generated by the SAMtools software (http://samtools.sourceforge.net/pileup.shtml). True RNA-editing events and exclusion of false positives was achieved by: 1) Mapping and base quality thresholds of 20 and 25, respectively; 2) a minimum coverage of 10 reads, of which at least 3 contain the variation; 3) a P value lower than 0.05 for FDR for REDItoolDenovo.py (Benjamini) and Fisher's exact test for VarScan; and 4) minimum editing frequency of 0.01. Annotation was performed using the ANNOVAR software (http://annovar.openbioinformatics.org/en/latest/) (69) providing dbSNP v142. Strand information was extracted from ENSEMBL.gtf files (mouse gene set) and annotated using custom R scripts and the refGenome R package. SNP exclusion, strand selection, and further statistical analysis for extracting and processing possible C-to-U and A-to-I RNA-editing events was performed using custom R scripts (procedure summarized in *SI Appendix*, Fig. S5). A github repository containing the in-house scripts used can be accessed through the link https://github.com/athanadd/CJD-mice.
Global RNA-editing profiles establishment and identification of differentially edited transcripts between control and sCJD animal groups. ADAR and APOBEC mediated RNA editing events predicted by Varscan and RedITools within each phenotype group (control, sCJD) and time point (120 dpi, 180 dpi) were used for establishing the corresponding ADAR and APOBEC mediated editomes. To minimize false-positive RNA-editing events, an arbitrary threshold value of 2 samples including a predicted RNA editing event within every sample group was set.

Acquired profiles were visualized by means of indexes depicting the distribution of editing events within each phenotype group per time point. Dual phenotype comparisons were performed on RNA-editing frequencies for each time point to identify statistically significant differences in RNA-editing frequency patterns between control and sCJD animals utilizing a 2-tailed unpaired Student's t test. P values of <0.05 were considered significant. As differentially edited were considered transcripts that were called by at least 1 of our bioinformatics suites, were detected in more than 50% of the animals of at least 1 of the studied phenotype groups and displayed editing frequencies ≥ 0.01 as well as $P \leq 0.05$ when dual phenotype comparisons were performed.
GO and pathway analysis. GO analysis utilizing the differential editome sets representative of each phenotype group and disease stage were performed using the DAVID 6.8 (https://david.ncifcrf.gov/) (70) software for identification of cellular processes and pathways affected by editing events.

RNA-Editing Validations. Reverse-transcription reactions were performed using 500 ng of total RNA and both the oligodT and random hexamer primers included in the PrimeScript kit (TAKARA), following the manufacturer's instructions. Amplification of an 800- to 900-bp transcript region including the positions of interest was performed using the prepared cDNAs and the high-fidelity Q5 DNA polymerase (New England Biolabs), according to the manufacturer's instructions. Primer sequences for each target are provided in *SI Appendix*, Table S9. In cases where editing events were predicted to be present in 1 of the tested groups (*Fkrp*, *Plekhm2*, and *Sec61a1*), PCR products were directly sequenced following PCR clean-up (PCR clean-up and gel-extraction kit, Macherey-Nagel). In cases where editing events were predicted to be present in both groups (*Sidt2*, *CTSS*, *B2M*, and *PAQR8*), a further step of TA cloning was applied before sequencing analysis. For cloning in the pDrive vector (Qiagen), PCR products were subjected to an additional A-tailing step, followed by clean-up and ligation in the pDrive vector using a 20× excess molar ratio of insert relative to the vector. Plasmids corresponding to 30 clones of transformed TOP10 *Escherichia coli* cells in each case were prepared using the Nucleospin plasmid kit (Macherey-Nagel) and sequenced at both directions. All sequencing reactions were performed by Cemia (https://cemia.eu/) using the v3.1 BigDye Terminator chemistry (ABI) and were analyzed on a 3730 genetic analyzer (ABI). Raw sequencing data were processed with the Bioedit software v7.09.0. RDDs corresponding to RNA-editing events were identified through alignment of cDNA sequencing data with the corresponding reference sequence. Murine and human genomic DNA regions corresponding to the candidate targets were also amplified, sequenced and used as reference sequences for RDDs identification.

1. G. Puoti *et al.*, Sporadic human prion diseases: Molecular insights and diagnosis. *Lancet Neurol.* **11**, 618–628 (2012).
2. U. Heinemann *et al.*, Creutzfeldt-Jakob disease in Germany: A prospective 12-year surveillance. *Brain* **130**, 1350–1359 (2007).
3. W. Xiang *et al.*, Identification of differentially expressed genes in scrapie-infected mouse brains by using global gene expression technology. *J. Virol.* **78**, 11051–11060 (2004).
4. P. J. Skinner *et al.*, Gene expression alterations in brains of mice infected with three strains of scrapie. *BMC Genomics* **7**, 114 (2006).
5. Y. Tang, W. Xiang, S. A. C. Hawkins, H. A. Kretzschmar, O. Windl, Transcriptional changes in the brains of cattle orally infected with the bovine spongiform encephalopathy agent precede detection of infectivity. *J. Virol.* **83**, 9464–9473 (2009).
6. M. Barbisin *et al.*, Gene expression profiling of brains from bovine spongiform encephalopathy (BSE)-infected cynomolgus macaques. *BMC Genomics* **15**, 434 (2014).
7. F. Llorens *et al.*, Subtype and regional-specific neuroinflammation in sporadic creutzfeldt-jakob disease. *Front. Aging Neurosci.* **6**, 198 (2014).
8. F. Llorens *et al.*, Altered Ca²⁺ homeostasis induces Calpain-Cathepsin axis activation in sporadic Creutzfeldt-Jakob disease. *Acta Neuropathol. Commun.* **5**, 35 (2017).
9. D. Hwang *et al.*, A systems approach to prion disease. *Mol. Syst. Biol.* **5**, 252 (2009).
10. A. Majer *et al.*, Early mechanisms of pathobiology are revealed by transcriptional temporal dynamics in hippocampal CA1 neurons of prion infected mice. *PLoS Pathog.* **8**, e1003002 (2012).
11. J. A. Carroll, J. F. Striebel, K. Race, K. Phillips, B. Chesebro, Prion infection of mouse brain reveals multiple new upregulated genes involved in neuroinflammation or signal transduction. *J. Virol.* **89**, 2388–2404 (2015).
12. A. R. Brown *et al.*, Gene expression profiling of the preclinical scrapie-infected hippocampus. *Biochem. Biophys. Res. Commun.* **334**, 86–95 (2005).

13. W. Xiang et al., Transcriptome analysis reveals altered cholesterol metabolism during the neurodegeneration in mouse scrapie model. J. Neurochem. 102, 834–847 (2007).

14. G. Sorensen et al., Comprehensive transcriptional profiling of prion infection in mouse models reveals networks of responsive genes. BMC Genomics 9, 114 (2008).

15. C. Riemer et al., Gene expression profiling of scrapie-infected brain tissue. Biochem. Biophys. Res. Commun. 323, 556–564 (2004).

16. W. Xiang et al., Cerebral gene expression profiles in sporadic Creutzfeldt-Jakob disease. Ann. Neurol. 58, 242–257 (2005).

17. C. Tian et al., Analyses of the similarity and difference of global gene expression profiles in cortex regions of three neurodegenerative diseases: Sporadic Creutzfeldt-Jakob disease (sCJD), fatal familial insomnia (FFI), and Alzheimer's disease (AD). Mol. Neurobiol. 50, 473–481 (2014).

18. M. Singh, Dysregulated A to I RNA editing and non-coding RNAs in neurodegeneration. Front. Genet. 3, 326 (2013).

19. K. Khermesh et al., Reduced levels of protein recoding by A-to-I RNA editing in Alzheimer's disease. RNA 22, 290–302 (2016).

20. S. Maas, A. Rich, Changing genetic information through RNA editing. Bioessays 22, 790–802 (2000).

21. P. Kiesel, W. Bodemer, T. Gibson, H. Zischler, F. J. Kaup, Prion infected rhesus monkeys to study differential transcription of Alu DNA elements and editing of Alu transcripts in neuronal cells and blood cells. J. Med. Primatol. 41, 176–182 (2012).

22. J. A. Carroll et al., Prion strain differences in accumulation of PrPSc on neurons and glia are associated with similar expression profiles of neuroinflammatory genes: Comparison of three prion strains. PLoS Pathog. 12, e1005551 (2016).

23. A. A. Asuni, M. Guridi, S. Sanchez, M. J. Sadowski, Antioxidant peroxiredoxin 6 protein rescues toxicity due to oxidative stress and cellular hypoxia in vitro, and attenuates prion-related pathology in vivo. Neurochem. Int. 90, 152–165 (2015).

24. C. Zhu et al., Triggering receptor expressed on myeloid cells-2 is involved in prion-induced microglial activation but does not contribute to prion pathogenesis in mouse brains. Neurobiol. Aging 36, 1994–2003 (2015).

25. L. Qiao et al., Lysosomal enzyme cathepsin D protects against alpha-synuclein aggregation and toxicity. Mol. Brain 1, 17 (2008).

26. G. Kaur, E. Levy, Cystatin C in Alzheimer's disease. Front. Mol. Neurosci. 5, 79 (2012).

27. S. H. Lee et al., Identification of diverse adenosine-to-inosine RNA editing subtypes in colorectal cancer. Cancer Res. Treat. 49, 1077–1087 (2017).

28. L. Han et al., The genomic landscape and clinical relevance of A-to-I RNA editing in human cancers. Cancer Cell 28, 515–528 (2015).

29. L. Han, H. Liang, RNA editing in cancer: Mechanistic, prognostic, and therapeutic implications. Mol. Cell. Oncol. 3, e1117702 (2015).

30. N. Paz-Yaacov et al., Elevated RNA editing activity is a major contributor to transcriptomic diversity in tumors. Cell Rep. 13, 267–276 (2015).

31. V. Rayon-Estrada, F. N. Papavasiliou, D. Harjanto, RNA editing dynamically rewrites the cancer code. Trends Cancer 1, 211–212 (2015).

32. P. K. Srivastava et al., Genome-wide analysis of differential RNA editing in epilepsy. Genome Res. 27, 440–450 (2017).

33. T. Hwang et al., Dynamic regulation of RNA editing in human brain development and disease. Nat. Neurosci. 19, 1093–1099 (2016).

34. I. Gaisler-Salomon et al., Hippocampus-specific deficiency in RNA editing of GluA2 in Alzheimer's disease. Neurobiol. Aging 35, 1785–1791 (2014).

35. P. Danecek et al., High levels of RNA-editing site conservation amongst 15 laboratory mouse strains. Genome Biol. 13, 26 (2012).

36. D. C. Cole et al., Loss of APOBEC1 RNA-editing function in microglia exacerbates age-related CNS pathophysiology. Proc. Natl. Acad. Sci. U.S.A. 114, 13272–13277 (2017).

37. V. Blanc et al., Genome-wide identification and functional analysis of Apobec-1-mediated C-to-U RNA editing in mouse small intestine and liver. Genome Biol. 15, R79 (2014).

38. B. R. Rosenberg, C. E. Hamilton, M. M. Mwangi, S. Dewell, F. N. Papavasiliou, Transcriptome-wide sequencing reveals numerous APOBEC1 mRNA-editing targets in transcript 3′ UTRs. Nat. Struct. Mol. Biol. 18, 230–236 (2011).

39. M. A. Hassan, V. Butty, K. D. C. Jensen, J. P. J. Saeij, The genetic basis for individual differences in mRNA splicing and APOBEC1 editing activity in murine macrophages. Genome Res. 24, 377–389 (2014).

40. K. J. Hilton, C. Cunningham, R. A. Reynolds, V. H. Perry, Early hippocampal synaptic loss precedes neuronal loss and associates with early behavioural deficits in three distinct strains of prion disease. PLoS One 8, e68062 (2013).

41. C. Cunningham et al., Synaptic changes characterize early behavioural signs in the ME7 model of murine prion disease. Eur. J. Neurosci. 17, 2147–2155 (2003).

42. S. Y. Shim, S. Karri, S. Law, H. M. Schatzl, S. Gilch, Prion infection impairs lysosomal degradation capacity by interfering with rab7 membrane attachment in neuronal cells. Sci. Rep. 6, 21658 (2016).

43. D. Khatter et al., The small GTPase Arl8b regulates assembly of the mammalian HOPS complex on lysosomes. J. Cell Sci. 128, 1746–1761 (2015).

44. G. Jialin, G. Xuefan, Z. Huiwen, SID1 transmembrane family, member 2 (Sidt2): A novel lysosomal membrane protein. Biochem. Biophys. Res. Commun. 402, 588–594 (2010).

45. S. Aizawa et al., Lysosomal putative RNA transporter SIDT2 mediates direct uptake of RNA by lysosomes. Autophagy 12, 565–578 (2016).

46. K. Uchiyama et al., Prions disturb post-Golgi trafficking of membrane proteins. Nat. Commun. 4, 1846 (2013).

47. E. A. Alvarez-Miranda, M. Sinnl, H. Farhan, Alteration of Golgi structure by stress: A link to neurodegeneration? Front. Neurosci. 9, 435 (2015).

48. A. Beck et al., Identification of Sidt2 as a lysosomal cation-conducting protein. FEBS Lett. 591, 76–87 (2017).

49. C. Hetz, M. Russelakis-Carneiro, K. Maundrell, J. Castilla, C. Soto, Caspase-12 and endoplasmic reticulum stress mediate neurotoxicity of pathological prion protein. EMBO J. 22, 5435–5445 (2003).

50. M. Boonen et al., Cathepsin D and its newly identified transport receptor SEZ6L2 can modulate neurite outgrowth. J. Cell Sci. 129, 557–568 (2016).

51. R. Zimmermann, L. Müller, B. Wullich, Protein transport into the endoplasmic reticulum: Mechanisms and pathologies. Trends Mol. Med. 12, 567–573 (2006).

52. J. R. Lowry, A. Klegeris, Emerging roles of microglial cathepsins in neurodegenerative disease.. Brain Res. Bull. 139, 144–156 (2018).

53. D. Haves-Zburof et al., Cathepsins and their endogenous inhibitors cystatins: Expression and modulation in multiple sclerosis. J. Cell Mol. Med. 15, 2421–2429 (2011).

54. I. Schechter, E. Ziv, Cathepsins S, B and L with aminopeptidases display β-secretase activity associated with the pathogenesis of Alzheimer's disease. Biol. Chem. 392, 555–569 (2011).

55. Y. Sancak et al., The Rag GTPases bind raptor and mediate amino acid signaling to mTORC1. Science. 320, 1496–1501 (2008).

56. I. C. Nnah et al., TFEB-driven endocytosis coordinates MTORC1 signaling and autophagy. Autophagy 15, 151–164 (2019).

57. T. E. Welty, Juvenile myoclonic epilepsy: Epidemiology, pathophysiology, and management. Paediatr. Drugs 8, 303–310 (2006).

58. F. Llorens et al., Subtype and regional regulation of prion biomarkers in sporadic Creutzfeldt-Jakob disease. Neuropathol. Appl. Neurobiol. 41, 631–645 (2015).

59. F. Llorens et al., PrP mRNA and protein expression in brain and PrP(c) in CSF in Creutzfeldt-Jakob disease MM1 and VV2. Prion 7, 383–393 (2013).

60. D. Padilla et al., Sheep and goat BSE propagate more efficiently than cattle BSE in human PrP transgenic mice. PLoS Pathog. 7, e1001319 (2011).

61. L. Lam et al., Epigenetic changes in T-cell and monocyte signatures and production of neurotoxic cytokines in ALS patients. FASEB J. 30, 3461–3473 (2016).

62. A. Dobin et al., STAR: Ultrafast universal RNA-seq aligner. Bioinformatics 29, 15–21 (2013).

63. M. I. Love, W. Huber, S. Anders, Moderated estimation of fold change and dispersion for RNA-seq data with DESeq2. Genome Biol. 15, 550 (2014).

64. G. Ramaswami et al., Accurate identification of human Alu and non-Alu RNA editing sites. Nat. Methods 9, 579–581 (2012).

65. R. Soundararajan et al., Detection of canonical A-to-G editing events at 3′ UTRs and microRNA target sites in human lungs using next-generation sequencing. Oncotarget 6, 35726–35736 (2015).

66. D. Kim et al., TopHat2: Accurate alignment of transcriptomes in the presence of insertions, deletions and gene fusions. Genome Biol. 14, R36 (2013).

67. E. Picardi, G. Pesole, REDItools: High-throughput RNA editing detection made easy. Bioinformatics 29, 1813–1814 (2013).

68. D. C. Koboldt et al., VarScan: Variant detection in massively parallel sequencing of individual and pooled samples. Bioinformatics 25, 2283–2285 (2009).

69. K. Wang, M. Li, H. Hakonarson, ANNOVAR: Functional annotation of genetic variants from high-throughput sequencing data. Nucleic Acids Res. 38, e164 (2010).

70. W. Huang, B. T. Sherman, R. A. Lempicki, Systematic and integrative analysis of large gene lists using DAVID bioinformatics resources. Nat. Protoc. 4, 44–57 (2009).

NEUROSCIENCE